HHS Public Access

Author manuscript

Nanotechnology. Author manuscript; available in PMC 2016 May 08.

Published in final edited form as:

Nanotechnology. 2015 May 8; 26(18): 185101. doi:10.1088/0957-4484/26/18/185101.

Carbon Nanoelectrodes for Single-Cell Probing

Sean E. Anderson and **Haim H. Bau***

University of Pennsylvania, Department of Mechanical Engineering and Applied Mechanics, Philadelphia, PA 19104

Abstract

Carbon nanoelectrodes with tip diameters ranging from tens to hundreds of nm are fabricated by pyrolitic deposition of carbon films along the entire inner surfaces of pulled-glass pipettes. The pulled end of each glass pipette is then etched to expose a desired length (typically, a few μm) of carbon pipe. The carbon film provides an electrically conductive path from the nanoscopic carbon tip to the distal, macroscopic end of the pipette, bridging between the nanoscale tip and the macroscale handle, without a need for assembly. We used our nanoelectrodes to penetrate into individual cells and cell nuclei and measured the variations in the electrode impedance upon cell and nucleus penetration as well as the electrode impedance as a function of cell penetration depth. Theoretical predictions based on a simple circuit model were in good agreement with experimental data.

Keywords

carbon nanopipettes (CNP); nano; probe; electrode; biosensing; cell; single; electrochemical methods

Introduction

In recent years, there has been a growing interest in studying single cells to better understand cellular and sub-cellular processes that otherwise may be obscured by cells' heterogeneity. Micro- and nano-electrodes are effective tools for such studies since they are minimally invasive, causing small system perturbation, and provide fast time response, high spatial resolution, small ohmic potential drop compared to sharp electrodes (micropipettes containing electrolyte solution), and improved signal to noise ratio.[1] Micro and nano electrodes can be used to detect various electrochemically-active, biologically-important species, such as catecholamines (neurotransmitters), oxygen, nitric oxide, reactive oxygen species (ROS), and reactive nitrogen species (RNS), under physiological conditions.[2] Advancements in micro/nanoelectrode fabrication methods[3–7], improvements in measurement techniques,[8–12] and novel surface functionalizations[8, 13, 14] are providing opportunities to study various single-cell characteristics[15, 16].

*Corresponding Author: bau@seas.upenn.edu.

Author Contributions

The research presented in this paper was performed by Sean E. Anderson under the advisement of Prof. Haim H. Bau. SEA performed the experiments; SEA and HHB designed the experiments, discussed the results, and wrote the paper.

Until recently, most electrochemical measurements of single-cells have been carried out with sensors positioned in the extracellular solution to monitor, among other things, cellular respiration and exocytosis of neurotransmitters, carry out scanning electrochemical microscopy (SECM), and form patch-clamps to probe ionic channels.[17–27] Sharp-like electrodes with ohmic conductivity that can carry out electrochemical measurements inside the cell and in organelles provide new opportunities.[21]

Carbon nanopipettes (CNPs) are one example of an intracellular probe. The CNPs consist of a pulled-quartz micropipette with a thin film of amorphous carbon selectively deposited along the pipette's *entire* interior surface *via* chemical vapor deposition.[3–5] The tip of the glass is then etched to expose a carbon pipe with a diameter that can be controllably made in the range from tens to hundreds of nm (Fig. 1). The thin carbon film provides an electrically conductive path from the nanoscale tip to the macroscopic distal end of the CNP. See Fig. 1A for a schematic depiction and Figs. 1B and 1C for SEM micrographs. One significant advantage of the CNP is that it provides a means of interfacing a nanoscopic structure (the carbon nanopipe) with a macroscopic handle without a need for any assembly. The CNP can be made either hollow (Fig. 1A-i) to enable injection of reagents or completely sealed (Fig. 1A-ii) with carbon to provide a solid nanoelectrode. The CNP tip's diameter, exposed length, and taper are controllable and determined by process conditions. To date, unfunctionalized CNPs have been used for cell[28, 29] and nematode[30] microinjection, cell electrophysiology[31], fast-scan cyclic voltammetry to monitor neurotransmitter release and uptake in the brain of the fruit fly[32], and scanning electrochemical microscopy.[33] The surface of the tip of the CNP has also been functionalized with gold nanoparticles[34] to enable the binding of various ligands and enhance surface Raman emission[35].

Previously, we used a digital lock-in amplifier to measure variations in the liquid-filled CNP's interfacial impedance during penetration and microinjection into adherent mammalian cells.[29] Cell penetration detection is useful, among other things, to trigger cell injection in automated injection systems. In the above application, the CNP was filled with the liquid to be injected. As a result, there was a large interfacial area between the pipette's inner, carbon-coated, conductive surface and the electrolyte confined inside the CNP. Since upon cell penetration, the liquid confined in the pipette was completely isolated from the extracellular solution, a relatively large change in impedance was measured when the CNP traversed from the extracellular solution into the cytoplasm. In the above application, the CNP operated as a hybrid between a sharp and an ohmic electrode. The use of a lock-in amplifier allowed us to filter out noise and achieve high resolution on the order of femto-Farads (10^{-15}). In contrast, in this paper, we explore the feasibility of employing the lock-in amplifier to carry out measurements with a completely ohmic nanoelectrode. Although we can make the CNPs solid (Fig. 1A-ii) by running the carbon deposition process for a sufficiently long time to seal the carbon tip, the electrodes used in this paper were hollow (Fig. 1A-i). We prevented liquid imbibitions into the hollow of the CNP by applying backpressure. By varying the backpressure, we also explored the effects of partial liquid filling on probe's response.

The use of ohmic nanoelectrodes for single cell studies has attracted a considerable interest in recent years. SECM probes have been used to map cells' surface topography with

submicron resolution.[1, 11, 12, 20, 21, 33] Electrochemical impedance spectroscopy has been utilized to detect the binding of target analytes to selectively functionalized surfaces.[8, 13, 14] Capacitive measurements are especially useful for biodetection in the absence of Faradaic currents. Oxygen, a natural redox species, is present in our system, but does not contribute significantly to the Faradaic current at the potentials used in our experiments[36] and does not provide significant contrast between intra/extracellular environments due to its free diffusion across the cellular membrane. Carbon microelectrodes have been used in neuroscience for amperometric detection of neurotransmitter exocytosis and for fast scan cyclic voltammetry (FSCV) to monitor specific neurotransmitter concentrations with high temporal and spatial resolutions.[6, 7, 23–27, 32, 37] CNPs hold much promise for the above listed applications due to their small size, high spatial resolution, tunable dimensions, easy fabrication, and amenability to interfacing with standard electrophysiology and cell injection equipment.[3–5, 28, 29, 31]

Here, using lock-in amplifier, we measured variations of the interfacial impedance of the dry CNP as it penetrates into adherent mammalian cells and into cell nuclei. We also measured the CNP impedance as a function of the cell penetration depth and compared the experimental data with theoretical predictions based on a simple circuit model. Furthermore, we explored the effects of partial liquid filling on the CNP's impedance. This technique may be useful for positioning nanoelectrodes at desired positions for intracellular probing.

Experimental Section

Cell Culture and Imaging

The experiments were carried out with adherent human osteosarcoma cells (U2OS, ~40 μm diameter) plated on either Poly-L-Lysine treated glass coverslips or cell culture dishes. Imaging and recording were carried out, respectively, with an inverted Olympus IX-71 microscope with a long working distance, phase contrast objectives and a Hammamatsu ORCA-ER charge-coupled device (CCD) camera. The microscope was enclosed in a custom made copper-mesh Faraday cage and located on a TMC vibration-isolating table.

CNP Fabrication

The CNPs were fabricated according to protocols previously described.[3–5] Briefly, the dimensions of the CNP's tip were determined by process conditions. The outer carbon tip dimensions were dictated by the dimensions of the pulled glass pipette that served as a template. The glass pipette shape and dimensions were determined by the puller's program (Sutter Inc.). The carbon film thickness was determined by the duration of the CVD deposition time, the type and concentration of the precursor gas, and the process temperature. Typically, we selected temperatures that resulted in selective deposition inside the pipette and no deposition on the pipette's outer surface.[4, 5] Subsequent to the CVD process, the tip of the glass capillary was etched with Buffer HF Improved (Transene Inc.). The duration of the etching dictated the length of the exposed carbon pipe. For the work presented here, CNPs were fabricated with a tip outer diameters ranging from 200 to 400 nm, inner diameters ranging from 50 to 200 nm, and exposed carbon tip length ranging from 4 to 20 μm. The tip had a conical shape with a cone angle of 1.6 degrees on average. Fig. 1B

is a SEM image of a hollow CNP's tip with an outer diameter of 500nm. Witness the interface between the exposed carbon tip and the quartz pipette (highlighted with a dashed line). Fig. 1C is SEM image of a long exposed carbon tip with a 50nm tip diameter. The electrical resistance of the CNPs was on the order of tens of kΩ, which is negligible compared to the junction impedance of the electrode/electrolyte interface. When in solution, the DC junction impedance was on the order of 5GΩ, as measured by impedance spectroscopy. At 1 kHz in a typical cell medium, the interfacial impedance dropped to 10–100 MΩ.

Capacitance and Impedance Measurements

The CNPs were connected to a HEKA EPC 10 patch clamp amplifier and Eppendorf Femtojet pressure-injection pump with a standard 1.0mm HEKA pipette fitting. The pump has a dynamic range of 0–6000hPa (0–600kPa) with a resolution of 1hPa. The impedance was monitored in real time with the digital LockIn module of HEKA's PATCHMASTER software. The LockIn module recorded the current response to 10mV amplitude (20mV peak-peak), 1kHz sinusoidal potential perturbation. The current response was used to compute the complex impedance and the equivalent capacitance of the system. A silver/silver-chloride wire was inserted in the extracellular solution and used as a reference and counter electrode. The surface area of the reference/counterelectrode was sufficiently large (>1000× the CNP working electrode's area) to have a negligible contribution to the system's impedance, enabling a two-electrode measurements (since the currents were not sufficiently large to significantly alter the reference potential of the counterelectrode). The patch clamp amplifier headstage had a 0.5GΩ input impedance (for the gain setting used in our experiments).

Micromanipulation and Cell Experiments

The headstage of the amplifier was mounted on a piezoelectric micromanipulator (Eppendorf Transferman NK2). The CNP tip was brought into focus when ~50 μm above the cell. The pipette was then slowly lowered, and the scope was refocused until the CNP was visible several microns above the cell of interest. The background pressure in the pipette was adjusted to 3000–4000 hPa to minimize capillary imbibition. The signal stabilized within a few minutes of the application of the background pressure. This time constant is associated with the time required to eject any fluid that was uptaken by capillary rise in the hollow of the CNP. At pressures above 3000 hPa, the capacitance and impedance were pressure-independent, indicating complete expulsion of liquid from the inside of the pipette.

The CNP was manually lowered into the cell using the joystick on the piezomanipulator at <5μm/s and then halted upon cell or nucleus penetration. The impedance and capacitance were measured as functions of time. Cell penetration was confirmed visually. Upon contact with the cell, a cleft in the cell membrane created a contrast difference at the tip of the CNP, enhanced by the phase-contrast filters (Figs. 2A and 2B). Microinjection experiments of fluorescent dye verified that this visual clue does, indeed, indicate cell penetration.[29] The measured impedance change occurred simultaneously with the imaged penetration into the cell cytoplasm or the cell nucleus. Nuclei were clearly visible under the microscope. The instances of CNP penetration into and removal from the cell were recorded for each data

series. Data was exported to Matlab software (Mathworks Inc.) for analysis. Because the CNPs penetrated the cell rapidly and were typically held stationary after penetration, the signals often resembled step-changes. The data during the penetration was averaged and extracellular values were subtracted. The extracellular values before and after penetration were averaged to account for any drift.

To measure the impedance as a function of cell penetration depth, the CNP was brought into position above a cell and the micromanipulator was programmed to traverse at a constant speed of 400nm/s downwards with the pipette normal to the cell membrane. The resistance and capacitance were measured as functions of time. The time axis was then translated to the CNP tip's position. The data was exported to Matlab and was offset by the extracellular value to obtain the signal change as a function of depth. The manufacturer's specified step size is 40nm, and the manipulator traversed at 10 steps/s.

To study the effect of capillary rise inside the CNP, the extracellular capacitance value was measured as a function of CNP pressure.

Results and Discussion

In our experiments, we monitored the CNP's impedance as it penetrated into the cell. We start by describing a simple theoretical model that enables us to predict the CNP's impedance as a function of its tip position. Then, we compare the model predictions with experimental measurements.

A Simplified Circuit Model

To gain insights into our system's behavior, we use the equivalent circuit depicted in Fig. 1D. In contrast to our prior work,[29] the inner surface of the CNP is dry and not in contact with liquid. The symbols R and C denote, respectively, resistance and capacitance. The significance of the various subscripts and superscripts is delineated in the figure's caption. Briefly, the electrode-liquid interface is modeled as a Stern capacitor (C^S) in series with a Debye (diffuse) layer capacitor (C^d). These capacitors are connected in parallel with a Faradaic charge transfer resistor (R^t). Since, in our experiment, R^t is large, we can approximate the electrode as blocking (perfectly polarizable). Likewise, the membranes are approximated as capacitors with parallel resistances, corresponding to the ion channel conductance. Since the ion channel resistance is large compared to the capacitive impedance, we can approximate, to the first order, the entire circuit with capacitors alone. Figs. 1E and 1F depict, respectively the capacitance-based circuits for a CNP tip submerged in the extracellular solution and a CNP tip in the cytoplasm. Although the circuit still contains resistance components, the imaginary part of the impedance can be decoupled, with the measured capacitance of the whole system approximately equal to the equivalent capacitance of the capacitive elements, consisting of the double-layer and membrane capacitances alone. We calculated the probe capacitance when in the extracellular solution (Fig. 1E) and in the cytoplasm (Fig. 1F) using circuit theory.[38]

The capacitance change upon cell penetration

$$\Delta C_{eq} \sim \left\{ \frac{(C_i'' - C_o'')C_m - C_o'' C_i'' A_i}{C_i'' A_i + C_m} \right\} A_i \quad (1)$$

is the difference between the intracellular equivalent capacitance (Fig. 1F) and the extracellular equivalent capacitance (Fig. 1E). In the above, the double quotes denote capacitance per unit area. C_i", C_o", and C_m are, respectively, the specific surface capacitance when in contact with the cytoplasm, the specific surface capacitance when in contact with the extracellular solution, and the cell membrane capacitance. The change in capacitance is proportional to the area of the CNP's tip submerged inside the cell (A_i). Interestingly, depending on the relative magnitudes of C_o" and C_i", ΔC_{eq} can be either positive or negative. When the intracellular and extracellular solutions are nearly isotonic $(C_i'' \sim C_o'')$, equation (5) reduces to $\frac{-C_o'' C_i''}{C_i'' A_i + C_m} A_i^2 < 0$. This equation suggests that by monitoring the capacitance of an empty CNP, in addition to detecting cell penetration, we should be able to estimate the portion of the CNP's tip submerged in the cytoplasm and deduce from the known tip geometry, the penetration depth. This simplified, capacitance-based theory provides insights into many of our experimental observations. In our more complete numerical calculations, we included all circuit elements. The Matlab code to compute ΔC_{eq} that includes the contributions of the various resistances is available online.[39]

Cell Penetration Detection

When carrying out electrochemical measurements within cells, it is desirable to be able to determine when the probe crosses the cell membrane. In this section, we examine whether a capacitance measurement can serve as a robust indicator of cell penetration.

An empty CNP with an external tip diameter of 250 nm and an exposed tip length of 4 μm was mounted on the micromanipulator and connected to the patch-clamp amplifier and the microinjection pump. The pump pressure was maintained at 3000hPa (0.3 MPa) to exclude liquid penetration into the bore of the pipette. The backpressure is not needed when a solid probe is used.[32] Adherent Osteosarcoma cells (U2OS, ~40μm diameter) were plated on a glass slide and immersed in cell media (Dulbecco's Modified Eagle's Medium, supplemented with 10% Fetal Bovine Serum and 1% Penicillin/Streptomycin antibiotics). The micromanipulator was manually controlled and the tip position was imaged under the microscope. Each CNP's impedance was continuously monitored as the CNP was lowered into the cell.

Fig. 2 depicts typical experimental results during cell probing. Figures 2A and 2B depict micrographs of the sequences of CNP penetration into the cytoplasm (**A**) and nucleus (**B**). For better visibility, the CNP's tip is identified with an arrow and the cell nucleus is outlined in red in the first panel. Figure 2C depicts schematically the CNP tip's position in the extracellular solution (EC, corresponding to micrographs **2A(i)** and **2B(i)**), cell cytoplasm (C, corresponding to micrograph **2A(iii)**), and nucleus (N, corresponding to micrograph 2B(iii)). Fig. 2D depicts the measured equivalent capacitance C_{eq} as a function of time (and, indirectly, probe position) for penetration from the extracellular solution into the cytoplasm

and into the cell nucleus. Initially, the probe's tip traversed the extracellular solution and the equivalent capacitance remained nearly fixed. The low-pass filtered signal exhibited RMS (root mean square) fluctuations of about 2.0 fF. When the CNP's tip first touched the cell membrane, a dimple was observed in the membrane. At time t~5s, the CNP's tip penetrated through the cell membrane and C_{eq} dropped sharply by 23 fF. C_{eq} remained at this lower level as long as the CNP tip remained inside the cytoplasm. Once the tip was withdrawn from the cytoplasm (t~10s), the probe nearly regained its extracellular capacitance. At time t~20s, the probe was inserted into the cell's nucleus and the measured capacitance dropped by 49 fF from its extracellular value. Upon withdrawal to the extracellular medium (t~26s), the probe regained its extracellular capacitance. Witness the large difference between the capacitance changes (a factor of ~2) upon penetration into the cytoplasm and into the nucleus. The measured changes in capacitance are consistent with the predictions of our theoretical model. In the model, we used the characteristic values of cell membrane capacitance typical to U2OS cell. A CNP with 4μm exposed length, 1.6 degree cone angle, and 250 nm tip diameter is predicted to experience 23fF drop in capacitance when penetrating 2.6μm into the cytoplasm and 46fF drop in capacitance when penetrating 1.1μm into the model's cell nucleus. We assume that the entire 1.1μm of the CNP tip is within the cell nucleus and neglect any intermediary electrode interface between the nuclear and cell membranes. The nuclear membrane is conformal with the cell membrane in an adherent cell, and so this approximation is reasonable for modeling nuclear penetration.

Figure 2E (Top panel) depicts eight sequential probing events with the same CNP into the cytoplasm (C) and the nucleus (N) of different cells over a time interval of 120s. The penetration into the nucleus consistently resulted in a greater capacitance change than did the penetration into the cytoplasm, with average values (± one standard deviation) of $\Delta Ceq = -43.8\pm17.7$fF (nucleus, N=133), compared to -30.6 ± 17.4fF (cytoplasm, N=138). This difference was statistically significant using a large sample test for the difference between means, $P<0.0001$.[40]

Upon nucleus penetration and withdrawal, the capacitance signal occasionally featured sharp transient troughs (Figs. 2D and 2E). Although the cause of these troughs is not known with certainty, the relaxation time of these troughs of 0.3±0.04s (N=6) is consistent with the documented relaxation time associated with mechanical deformations of typical cells.[41] We hypothesize that during cell penetration, the CNP deformed the cytoskeleton and membrane. The transient peaks are likely associated with the time that it takes the cytoskeleton to recover its original state prior to cell penetration.

Figure 2F (Top panel) depicts the real part of the impedance, Re{Z}, as a function of time for the same penetration events shown in Fig. 2E. ΔC_{eq} was accompanied by a concurrent increase in the real part of the impedance, ΔRe{Z}. The ΔRe{Z} measurements had mean values (± one standard deviation) of 85.0±46.7kΩ (cytoplasm, N=138) and 86.9±87.1kΩ (nucleus, N=133), demonstrating relatively small difference between cytoplasm and nuclear probing and a large spread in the nuclear probing data. The difference between cytoplasmic and nuclear ΔRe{Z} was not statistically significant (P=0.59).

The lower panels of Figs. 2E and 2F are normalized time-derivatives of the data presented in the corresponding upper panels. The time derivatives were calculated by taking the difference between adjacent data points, using a 500 point (0.5s) moving average, and normalizing the difference with its maximum value. The spikes in the derivatives provide a convenient way to identify cell and nucleus penetration and retraction of the CNP from the nucleus and the cytoplasm. From the perspective of automation, a spike exceeding a pre-set threshold (i.e., the dashed lines in Figs. 2E and 2F) may be used to indicate cell or nucleus penetration and halt the manipulator's motion.

To discriminate between the signal changes due to contact with the substrate and cell penetration, we contacted the substrate lightly with the CNP tip in a region free of cells and measured the corresponding effect on the CNP's impedance (data not shown). In all cases, C_{eq} increased and Re{Z} decreased compared to their corresponding values in the extracellular solution. The reasons for these particular trends are not obvious and likely resulted from the CNP tip's bending when pushed against the substrate. The control experiments indicate, however, that the sign of the capacitance and resistance variations readily distinguishes between cell penetration and unintended contact with the substrate.

Slight drift and fluctuations both in the extracellular and intracellular measurements may have resulted from equipment vibrations, induction noise, capillary rise inside the CNP, physiological variations in the cell, and modifications in the electrode's surface due to fouling, and clogging. Indeed, the high sensitivity of the capacitance measurement to changes in the electrode interface's conditions can be used to detect CNP breakage and clogging as previously suggested.[29]

Despite having an electrode surface area much smaller than traditional microelectrodes, on the order of $10\mu m^2$, compared to microelectrodes' 10^2–$10^3\mu m^2$, a signal change was detected in all of the cell probing events, demonstrating that the CNPs can robustly and reliably detect cell penetration through capacitance measurement. The empty CNPs behave like ultra-micro electrodes (UME), albeit with the benefit of much greater spatial resolution and smaller intrusion.

Cytoplasm vs. Nucleus Penetration

When measuring CNP's equivalent capacitance during cell and nucleus penetration, we found a significant difference between the signal associated with cytoplasm penetration, $\Delta C_{eq,CP}$ (−30.6±17.4fF, N=138), and the signal associated with nuclear penetration, $\Delta C_{eq,N}$ (−43.8±17.7fF, N=133), P<0.0001. For the real part of the impedance, $\Delta Re\{Z\}_{CP}$=85.0±46.7kΩ (N=138) and $\Delta Re\{Z\}_{N}$=86.9±87.1kΩ (N=133) the difference was not significant. In the above, subscripts 'CP' and 'N' refer, respectively, to cytoplasm and nucleus. The ratio $\Delta C_{eq,N}/\Delta C_{eq,CP}$ ~ 1.4 while $\Delta Re\{Z\}_{N}/\Delta Re\{Z\}_{CP}$ ~1. The nuclear membrane does not significantly increase the real part of the impedance at the frequency used in our experiments.

Figs. 3A and 3B depict, respectively, the distributions of $\Delta C_{eq}^{1/2}$ associated with the penetration into the cytoplasm and into the nucleus. We selected to analyze the data in terms of $\Delta C_{eq}^{1/2}$ instead of ΔC_{eq} because the former could be better fitted with a Gaussian

distribution. We fit these probability distributions with Gaussian distributions (solid lines) with R^2 values of 0.93 (Cyto.) and 0.98 (Nuc.). Fig. 3C compares the probability distributions associated with cytoplasm and nucleus penetrations and shows them to be distinct ($P<0.0001$). The differences in $\Delta C_{eq,CP}$ and $\Delta C_{eq,N}$ are due to the nuclear membrane's impedance. Variations in the biological state of different cells, penetration depth of the CNP, and tolerances of the CNPs make it difficult to determine whether the tip is in the cytoplasm or nucleus based on a single impedance measurement, as is evident from the overlap of the distributions in Fig. 3C. When using a well-calibrated pipette and penetrating to a consistent depth, the signal magnitude can, however, be used to distinguish between cytoplasm and nuclear penetration.

Effect of Penetration Depth

To examine the change in the equivalent capacitance as a function of the CNP tip's penetration depth into the cell, we programmed the piezoelectric micromanipulator to traverse downwards at a uniform speed (400 nm/s) until after the cell was penetrated. The CNP impedance was continuously monitored during these experiments. Knowledge of the rate of descent allowed us to infer the distance travelled.

Fig. 4 depicts ΔC_{eq} (fF) of an empty CNP (hollow squares, backpressure of 4000hPa) contrasted with a CNP filled with extracellular solution (stars, ×0.1) as well as $\Delta \mathrm{Re}\{Z\}$ of an empty CNP (kΩ, upright triangles, 4000hPa backpressure) as functions of the CNP penetration depth (d μm) into the cytoplasm of a cell. The symbols and solid curves represent, respectively, experimental data and theoretical predictions. The error bars correspond to one standard deviation (N=10). To accommodate the data for the liquid-filled (stars) and empty (hollow squares) CNPs in the same graph, we multiplied the values of ΔC_{eq} associated with the liquid-filled CNP by the factor 0.1. At zero depth, the CNP's tip is fully in the extracellular solution. As d increases, the fraction of the exposed tip embedded in the cell, $|\Delta C_{eq}|$, and $\Delta \mathrm{Re}\{Z\}$ increase as well.

$|\Delta C_{eq}|$ and $\Delta \mathrm{Re}\{Z\}$ increased monotonically with the penetration depth (Fig. 4). We used the full network-based model[39] that includes the various resistances (Fig. 1D) to predict ΔC_{eq} and $\Delta \mathrm{Re}\{Z\}$ as functions of the penetration depth (solid lines). In the model, we used reported values of cell membrane capacitance[42] and resistance[43] and theoretical values for the diffuse layer capacitance based on Gouy-Chapmann-Stern (GCS) theory.[1] We modeled the CNP geometry as a simple truncated cone. The model for the empty CNP required just one fitting parameter: the CNP's Stern layer capacitance, which we estimated as $30 \mu F/cm^2$. This estimate is on the same order of magnitude as the documented[44] Stern layer capacitance of $40 \mu F/cm^2$ for a spherical microelectrode submerged in a KCl solution, and roughly half that predicted by GCS theory (~$65\ \mu F/cm^2$). In the case of the liquid-filled CNP, a second fitting parameter was needed to approximate the effective inner surface of the CNP in contact with the liquid. The theoretical predictions agree well with the experimental data (symbols). Consistent with our previous observations, the liquid-filled CNPs exhibited much greater $|\Delta C_{eq}|$ than the empty ones. The ability to estimate the CNP tip's penetration depth may be useful to minimize cell damage as well as to control the position of the electrode tip for intracellular sensing.

The simplified model for the capacitance variations (equation 1) approximates well the predictions of the full circuit model for Im{Z}. Although the increase in Re{Z} with penetration depth is consistent with intuition, we were not been able to come up with a simple model to predict Re{Z} as a function of d. Instead, we have to rely on the predictions of our full circuit model (Fig. 1D).

The spatial resolution of this technique depends on electrode geometry, amplifier characteristics, and the micromanipulator's resolution. Our micromanipulator step size limits our maximum resolution to 40nm and our amplifier noise level was measured to be 2.0fF. Once the probe is in the cytoplasm, we anticipate being able to detect penetration depth within 130nm. This estimate does not account for membrane indentation and possible cell remodeling during penetration. It is also important to appreciate the inherent variability of biological samples. Careful optimization and calibration would be necessary to use this technique in a quantitative (measuring penetration depth) rather than qualitative (detecting and minimizing penetration depth) manner.

Effect of Pressure on CNP Capillary Uptake

Since the carbon film inside the CNP is typically uninsulated from the liquid inside the CNP, the presence of liquid inside the CNP increases the electrode's effective area and affects the characteristics of the electrode. The hollow of the CNP may be completely or partially filled with solution. When an unpressurized, empty CNP is introduced into a solution, liquid will fill the hollow of the CNP by capillary imbibition. The electrode's increased interfacial area due to the presence of liquid in the CNP's hollow increases the EDL capacitance. Thus, when a liquid-filled CNP penetrates a cell, a much larger change in the equivalent capacitance is detected than when an empty CNP is used. The extent of the liquid imbibition into the CNP can be modified by adjusting the control pressure.

When control pressure is applied, this pressure counteracts the Laplace pressure at the fluid/air interface[45]

$$\Delta P = \frac{2\gamma}{r_b}, \quad (2)$$

where ΔP is the pressure difference across the interface (meniscus), γ is the surface tension, and r_b is the radius of the CNP's bore at the location of the interface. Since the capacitance change is proportional to the wetted area and the CNP's tip is conical, we expect $C_{eq} \sim 1/P^2$, where P is the control pressure. Below, we assume that only a part of the conical section of the CNP's bore is filled with solution. Fig. 5 depicts the measured C_{eq} as a function of $1/P^2$ for a characteristic CNP submerged in PBS buffer 1× (Hyclone). As expected, C_{eq} varies nearly linearly with $1/P^2$. Linear behavior with $1/P^2$ was consistent among all CNPs tested (N=5), with an average R^2 value of 0.96. When we extrapolate the data of Fig. 6 to $Pa \rightarrow \infty$, we find less than a 2% difference, on average (5 CNPs), between the extrapolated value of C_{eq} at $Pa \rightarrow \infty$, and the value at the working pressure. We consider the pressure sufficiently high to render capillary effects insignificant. This characterization could be useful in applications that require uptake of liquids by capillary action, for example in

electrochemical nanosamplers[46] or to characterize the internal geometry near the CNP's tip.

Conclusions

We have demonstrated the applicability of ohmic CNP nanoelectrodes for sub-micron cellular probing using AC potential and digital lock in methods without a need for redox mediators for signal enhancement and with millisecond time resolution. The CNPs can be readily mass produced and are compatible with standard cell electrophysiology and cell injection equipment, allowing easy adaptation. We measured variations in electrode capacitance upon penetration into the cytoplasm and the nucleus without reliance on the presence of a liquid in the CNP bore to increase the effective area of the electrode.

There were significant differences in signal magnitudes between nuclear and cytoplasmic penetration. The capacitance decreased and the resistance increased monotonically as functions of the cell penetration depth. Thus, one may be able to infer the CNP tip's position from the impedance measurement. The experimental data agreed well with theoretical predictions obtained with a simple equivalent circuit model. Appropriately functionalized nanoelectrodes can potentially be used for various intracellular biosensing applications.

Our work suggests yet another application of the CNPs, controllable sampling of sub-femtoliter liquid volumes. The liquid uptake can be controlled with back pressure and the liquid volume estimated with a capacitance measurement.

Acknowledgements

The work was supported, in part, by NIH grant 1R21EB016343-01 to the University of Pennsylvania, by the Commonwealth of Pennsylvania under the Ben Franklin Technology Development Authority and the Nanotechnology Institute, Department of Education GAANN program, Grant number P200A120237, and the NSF DMR08-32802, NSEC - Nano/Bio Interface Center. E. Brailoiu (Temple University) supplied the U2OS cell line used in our experiments and provided advice on cell culturing. J. Griepenberg, C. Lanci, and I. Dmochowski (University of Pennsylvania) provided access to their cell culture facilities. R. Singhal and Y. Gao (Drexel University) assisted with the CNP fabrication.

References

1. Bard, AJ.; Faulkner, LR. Electrochemical Methods: Fundamentals and Applications. Wiley; 2000.
2. Nebel M, Grutzke S, Diab N, Schulte A, Schuhmann W. Microelectrochemical visualization of oxygen consumption of single living cells. Faraday Discuss. 2013; 164:19–32. [PubMed: 24466656]
3. Kim BM, Murray T, Bau HH. The fabrication of integrated carbon pipes with sub-micron diameters. Nanotechnology. 2005; 16(8):1317–1320.
4. Schrlau MG, Falls EM, Ziober BL, Bau HH. Carbon nanopipettes for cell probes and intracellular injection. Nanotechnology. 2008; 19(1)
5. Singhal R, Bhattacharyya S, Orynbayeva Z, Vitol E, Friedman G, Gogotsi Y. Small diameter carbon nanopipettes. Nanotechnology. 2010; 21(1)
6. Huang WH, Pang DW, Tong H, Wang ZL, Cheng JK. A method for the fabrication of low-noise carbon fiber nanoelectrodes. Anal Chem. 2001; 73(5):1048–1052. [PubMed: 11289416]
7. Lin YQ, Trouillon R, Svensson MI, Keighron JD, Cans AS, Ewing AG. Carbon-Ring Microelectrode Arrays for Electrochemical Imaging of Single Cell Exocytosis: Fabrication and Characterization. Anal Chem. 2012; 84(6):2949–2954. [PubMed: 22339586]

8. Katz E, Willner I. Probing Biomolecular Interactions at Conductive and Semiconductive Surfaces by Impedance Spectroscopy: Routes to Impedimetric Immunosensors, DNA-Sensors, and Enzyme Biosensors. Electroanal. 2003; 15(11):913–947.
9. Gillis KD. Admittance-based measurement of membrane capacitance using the EPC-9 patch-clamp amplifier. Pflug Arch Eur J Phy. 2000; 439(5):655–664.
10. Chen P, Gillis KD. The noise of membrane capacitance measurements in the whole-cell recording configuration. Biophys J. 2000; 79(4):2162–2170. [PubMed: 11023920]
11. Amemiya S, Bard AJ, Fan FRF, Mirkin MV, Unwin PR. Scanning Electrochemical Microscopy. Annu Rev Anal Chem. 2008; 1:95–131.
12. Bergner S, Vatsyayan P, Matysik FM. Recent advances in high resolution scanning electrochemical microscopy of living cells - A review. Anal Chim Acta. 2013; 775:1–13. [PubMed: 23601970]
13. Randviir EP, Banks CE. Electrochemical impedance spectroscopy: an overview of bioanalytical applications. Anal Methods-Uk. 2013; 5(5):1098–1115.
14. Actis P, Mak AC, Pourmand N. Functionalized nanopipettes: toward label-free, single cell biosensors. Bioanalytical reviews. 2010; 1(2–4):177–185. [PubMed: 20730113]
15. Wang D, Bodovitz S. Single cell analysis: the new frontier in 'omics'. Trends in biotechnology. 2010; 28(6):281–290. [PubMed: 20434785]
16. Fritzsch FS, Dusny C, Frick O, Schmid A. Single-cell analysis in biotechnology, systems biology, and biocatalysis. Annual review of chemical and biomolecular engineering. 2012; 3:129–155.
17. Adams KL, Puchades M, Ewing AG. In Vitro Electrochemistry of Biological Systems. Annu Rev Anal Chem (Palo Alto Calif). 2008; 1:329. [PubMed: 20151038]
18. Amatore C, Arbault S, Bouton C, Coffi K, Drapier JC, Ghandour H, et al. Monitoring in real time with a microelectrode the release of reactive oxygen and nitrogen species by a single macrophage stimulated by its membrane mechanical depolarization. Chembiochem : a European journal of chemical biology. 2006; 7(4):653–661. [PubMed: 16502474]
19. Zhao Y, Inayat S, Dikin DA, Singer JH, Ruoff RS, Troy JB. Patch clamp technique: Review of the current state of the art and potential contributions from nanoengineering. Proceedings of the Institution of Mechanical Engineers, Part N: Journal of Nanoengineering and Nanosystems. 2008; 222(1):1–11.
20. Sun P, Laforge FO, Mirkin MV. Scanning electrochemical microscopy in the 21st century. Phys Chem Chem Phys. 2007; 9(7):802–823. [PubMed: 17287874]
21. Sun P, Laforge FO, Abeyweera TP, Rotenberg SA, Carpino J, Mirkin MV. Nanoelectrochemistry of mammalian cells. P Natl Acad Sci USA. 2008; 105(2):443–448.
22. Lindau M, Neher E. Patch-Clamp Techniques for Time-Resolved Capacitance Measurements in Single Cells. Pflug Arch Eur J Phy. 1988; 411(2):137–146.
23. Mellander L, Cans AS, Ewing AG. Electrochemical Probes for Detection and Analysis of Exocytosis and Vesicles. Chemphyschem. 2010; 11(13):2756–2763. [PubMed: 20737529]
24. Venton BJ, Wightman RM. Psychoanalytical electrochemistry: Dopamine and behavior. Anal Chem. 2003; 75(19):414A–421A.
25. Wang W, Zhang SH, Li LM, Wang ZL, Cheng JK, Huang WH. Monitoring of vesicular exocytosis from single cells using micrometer and nanometer-sized electrochemical sensors. Anal Bioanal Chem. 2009; 394(1):17–32. [PubMed: 19274456]
26. Cahill PS, Walker QD, Finnegan JM, Mickelson GE, Travis ER, Wightman RM. Microelectrodes for the measurement of catecholamines in biological systems. Anal Chem. 1996; 68(18):3180–3186. [PubMed: 8797378]
27. Wightman RM, May LJ, Michael AC. Detection of Dopamine Dynamics in the Brain. Anal Chem. 1988; 60(13):A769-&.
28. Schrlau MG, Brailoiu E, Patel S, Gogotsi Y, Dun NJ, Bau HH. Carbon nanopipettes characterize calcium release pathways in breast cancer cells. Nanotechnology. 2008; 19(32)
29. Anderson SE, Bau HH. Electrical detection of cellular penetration during microinjection with carbon nanopipettes. Nanotechnology. 2014; 25(24)

30. Brennan LD, Roland T, Morton DG, Fellman SM, Chung SY, Soltani M, et al. Small Molecule Injection into Single-Cell C. elegans Embryos via Carbon-Reinforced Nanopipettes. Plos One. 2013; 8(9)
31. Schrlau MG, Dun NJ, Bau HH. Cell Electrophysiology with Carbon Nanopipettes. Acs Nano. 2009; 3(3):563–568. [PubMed: 19309170]
32. Rees HR, Anderson SE, Privman E, Bau HH, Venton BJ. Carbon nanopipette electrodes for dopamine detection in Drosophila. Anal Chem. 2015
33. Hu KK, Gao Y, Wang YX, Yu Y, Zhao X, Rotenberg SA, et al. Platinized carbon nanoelectrodes as potentiometric and amperometric SECM probes. J Solid State Electr. 2013; 17(12):2971–2977.
34. Vitol EA, Schrlau MG, Bhattacharyya S, Ducheyne P, Bau HH, Friedman G, et al. Effects of Deposition Conditions on the Structure and Chemical Properties of Carbon Nanopipettes. Chem Vapor Depos. 2009; 15(7–9):204–208.
35. Singhal R, Orynbayeva Z, Sundaram RVK, Niu JJ, Bhattacharyya S, Vitol EA, et al. Multifunctional carbon-nanotube cellular endoscopes. Nat Nanotechnol. 2011; 6(1):57–64. [PubMed: 21151109]
36. Zachek MK, Takmakov P, Moody B, Wightman RM, McCarty GS. Simultaneous Decoupled Detection of Dopamine and Oxygen using Pyrolyzed Carbon Microarrays and FSCV. Anal Chem. 2009; 81(15):6258–6265. [PubMed: 19552423]
37. Rees HR, Anderson SE, Privman E, Bau HH, Venton BJ. Carbon nanopipette electrodes for dopamine detection in Drosophila.
38. Nilsson, JW.; Riedel, SA. Introductory Circuits for Electrical and Computer Engineering. Prentice Hall; 2002.
39. Anderson SE. GitHub - Carbon Nanoelectrodes for Single-Cell Probing - Circuit Simulation Code. 2014 Circuit Simulation. Available from: https://github.com/seanderson12/Carbon_Nanoelectrodes_for_Single_Cell_Probing.
40. Navidi, W. Statistics for Engineers and Scientists. McGraw-Hill Education; 2008.
41. Wong PK, Tan W, Ho CM. Cell relaxation after electrodeformation: effect of latrunculin A on cytoskeletal actin. J Biomech. 2005; 38(3):529–535. [PubMed: 15652551]
42. Hamill OP, Marty A, Neher E, Sakmann B, Sigworth FJ. Improved Patch-Clamp Techniques for High-Resolution Current Recording from Cells and Cell-Free Membrane Patches. Pflug Arch Eur J Phy. 1981; 391(2):85–100.
43. Johnson SL, Woodbury JW. Membrane Resistance of Human Red Cells. J Gen Physiol. 1964; 47(5):827-&. [PubMed: 14155431]
44. Wang HN, Pilon L. Accurate Simulations of Electric Double Layer Capacitance of Ultramicroelectrodes. J Phys Chem C. 2011; 115(33):16711–16719.
45. Berg, JC. An Introduction to Interfaces & Colloids: The Bridge to Nanoscience. World Scientific; 2010.
46. Yu Y, Noel JM, Mirkin MV, Gao Y, Mashtalir O, Friedman G, et al. Carbon Pipette-Based Electrochemical Nanosampler. Anal Chem. 2014; 86(7):3365–3372. [PubMed: 24655227]

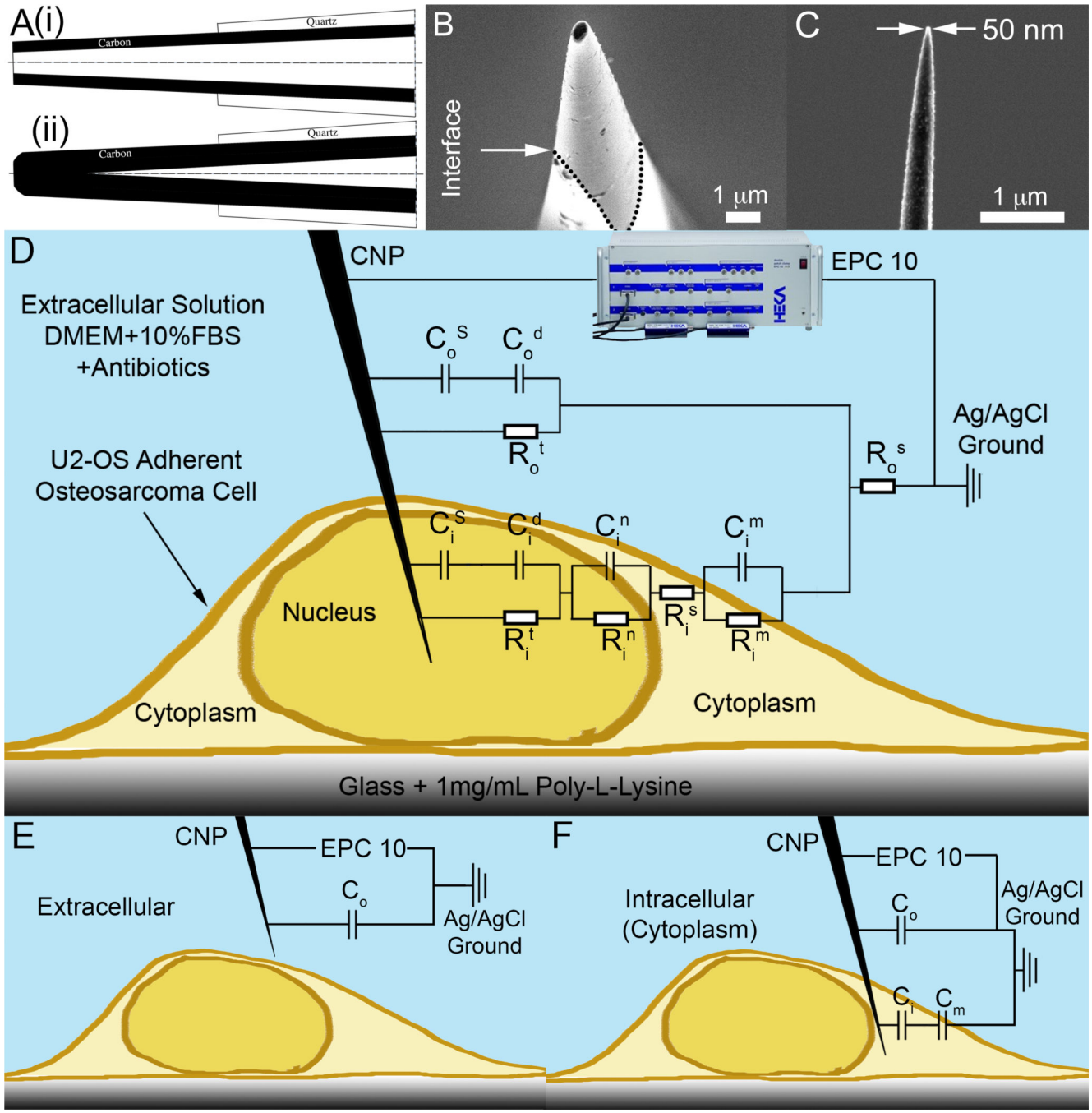

Figure 1.

Carbon Nanopipettes (CNPs) for cell probing. (A) A schematic depiction of the CNP's cross-section. (i) Open-tipped (hollow) CNP. (ii) Solid CNP. (B) A SEM side micrograph of a CNP's tip (500nm diameter, inclined at 10° off-axis). The quartz-carbon interface is delineated with dotted lines. (C) A SEM side view of a solid CNP with 50nm tip diameter. (D–F) A schematic depiction of a CNP penetrating an adherent cell with the equivalent circuit model overlaid. C and R denote, respectively, capacitors and resistors. Subscripts o, and i designate, respectively, extracellular and intracellular circuit components. Superscripts

designate the following: S - Stern layer (capacitance), s- series (resistance), d – diffuse layer, n – nuclear membrane, m – cellular membrane, t – charge transfer. When modeling cytoplasm probing, the nuclear circuit elements (C_i^n and R_i^n) are omitted. (D) Complete circuit model. (E) Extracellular circuit approximation, only capacitors are included. (F) Intracellular (cytoplasm) circuit approximation, only capacitors are included.

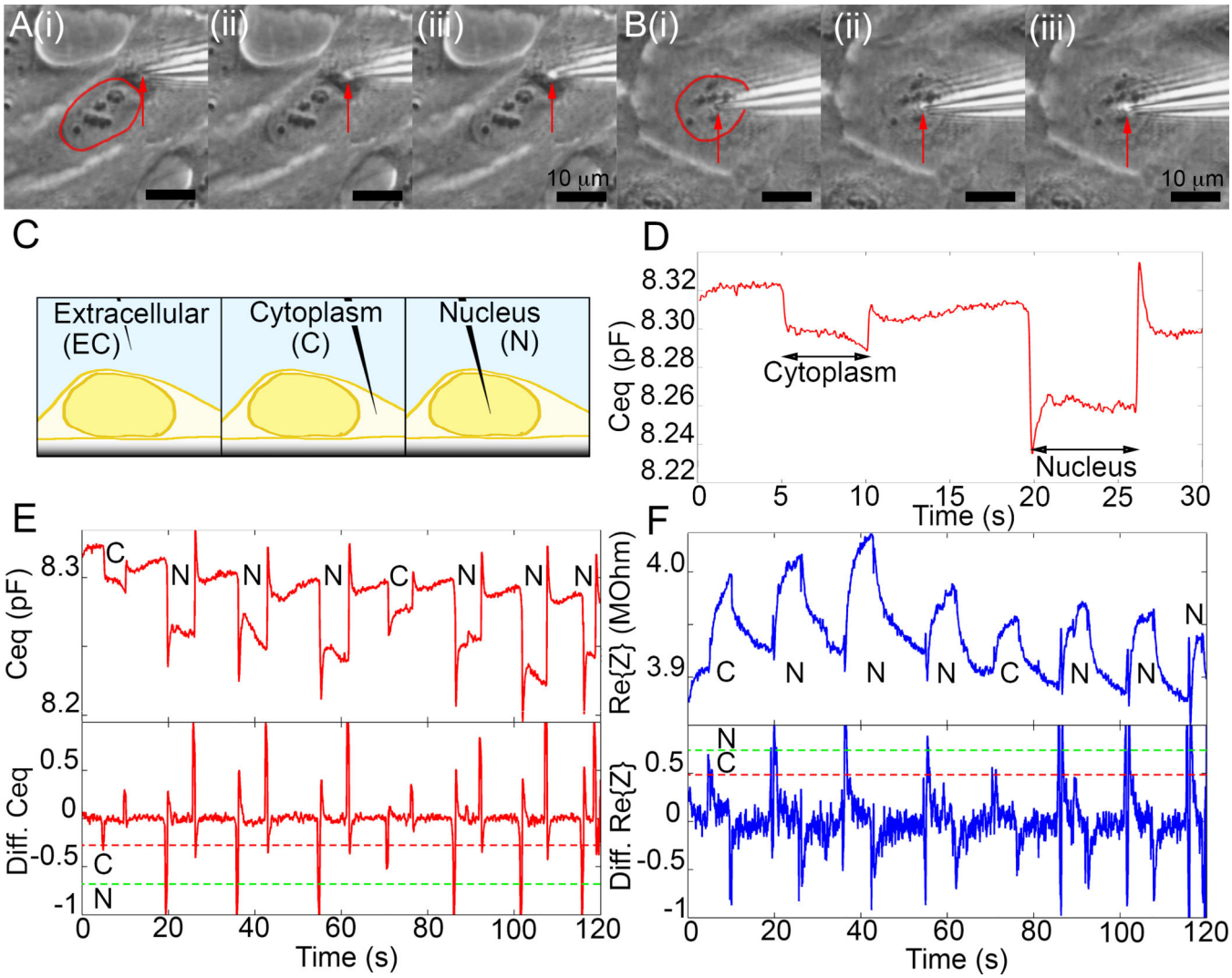

Figure 2.

Cell penetration impedance detection with an empty (pressurized to 3000hPa) CNP. (A) Micrographs of probing the cell cytoplasm. i) The CNP is outside of the cell, (the nucleus outlined with a red line). ii) The CNP has just contacted the cell membarne. iii) The CNP lowered into the cell. (B) Probing the cell nucleus. i) The CNP is outside of the cell, (the nucleus outlined with a red line). ii) The CNP has just contacted the cell. iii) The CNP has been lowered into the nucleus. Membrane contact/penetration is indicated by the bright spot at the pipette's tip due to the phase contrast filter, enhancing the contrast at the deformed membrane cleft. The CNP tip is identified with red arrows. Scale bar 10μm. (C) Schematics showing the CNP's tip positions: in the extracellular solution (EC, left), in the cell cytoplasm (C, middle), in the cell nucleus (N, right). (D) The measured capacitance as a function of time before, during, and after penetration into the cell cytoplasm and the nucleus. (E) The capacitance (Top) and the normalized capacitance time derivative (Bottom) as functions of time for cytoplasmic (C) and nuclear (N) probing events in different cells with the same CNP. (F) Re{Z} (Top) and its normalized time-derivative (Bottom) as functions of

time for the same probing events in panel C. The dashed lines in (E) and (F) represent possible threshold values for identifying cytoplasmic and nuclear penetration.

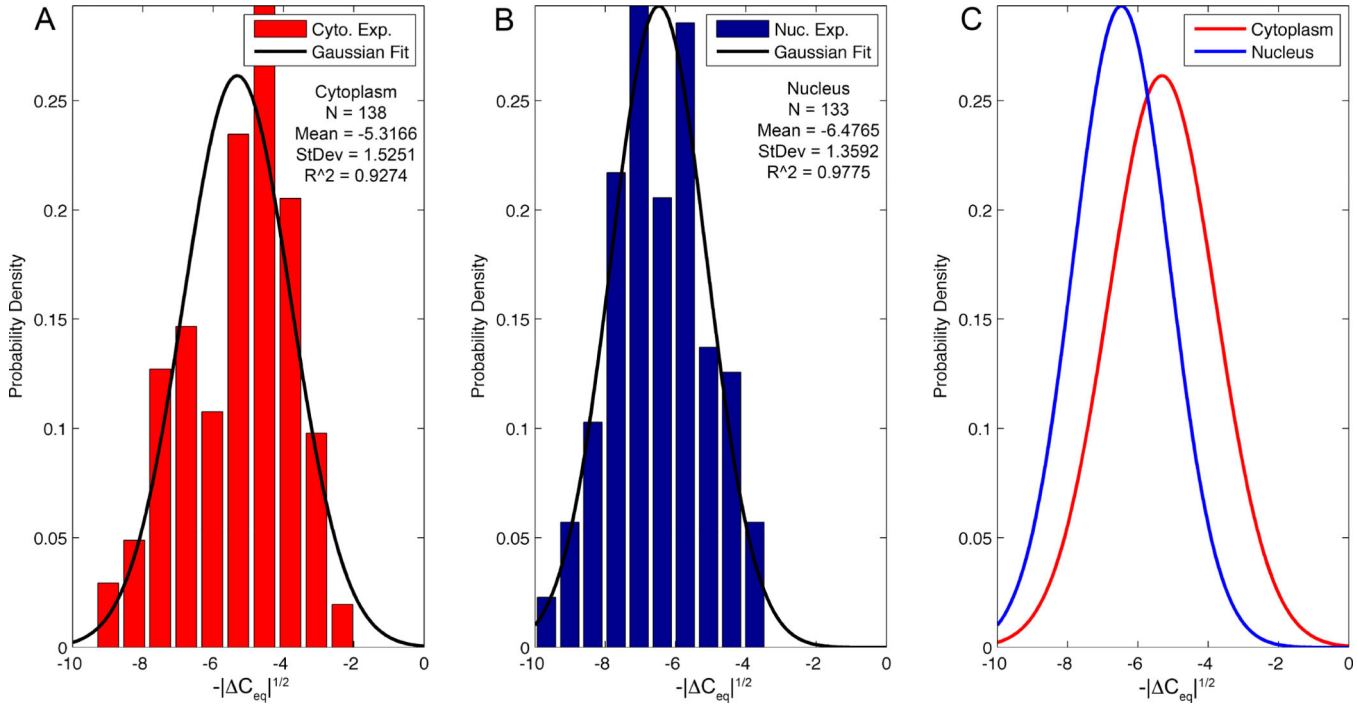

Figure 3.

Distribution histograms of cellular probing data (bars) for cytoplasm (N=138) (A) and nucleus (N=133) (B) with Gaussian fits (solid lines). (C) Comparison between the Gaussian fits from (A) and (B). The y-axis data is normalized to produce a probability density function and the x-axis is the square root of the capacitance change.

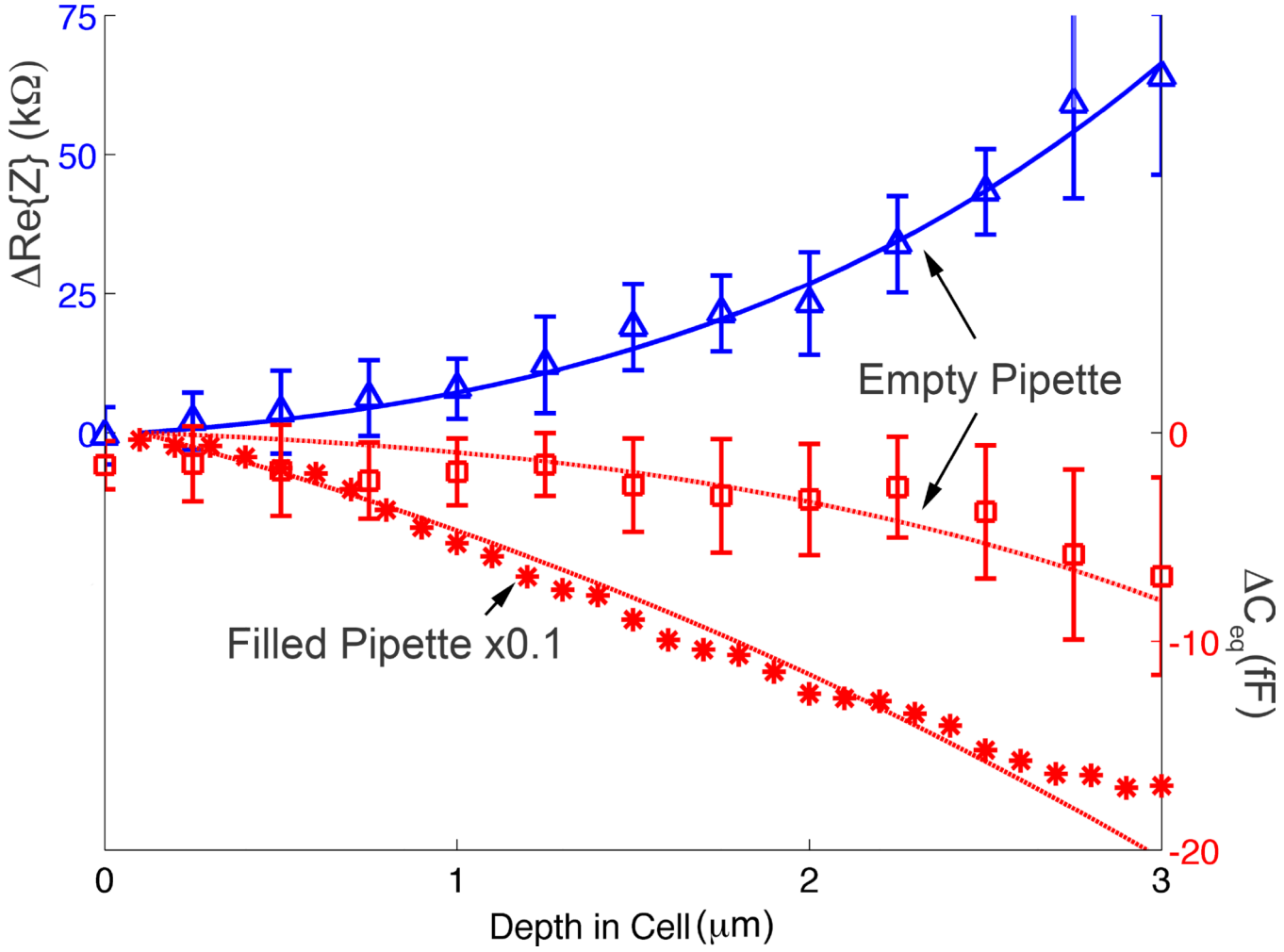

Figure 4.

The real part of the change in the impedance ΔRe{Z} (blue triangles, empty CNP, n=10), ΔC_{eq} (red hollow squares, empty CNP, N=10), and ΔC_{eq} (red stars, liquid-filled CNP, N=1) are depicted as functions of the cell penetration depth (d μm) into the cytoplasm. The symbols and lines represent, respectively, experimental data and theoretical predictions.

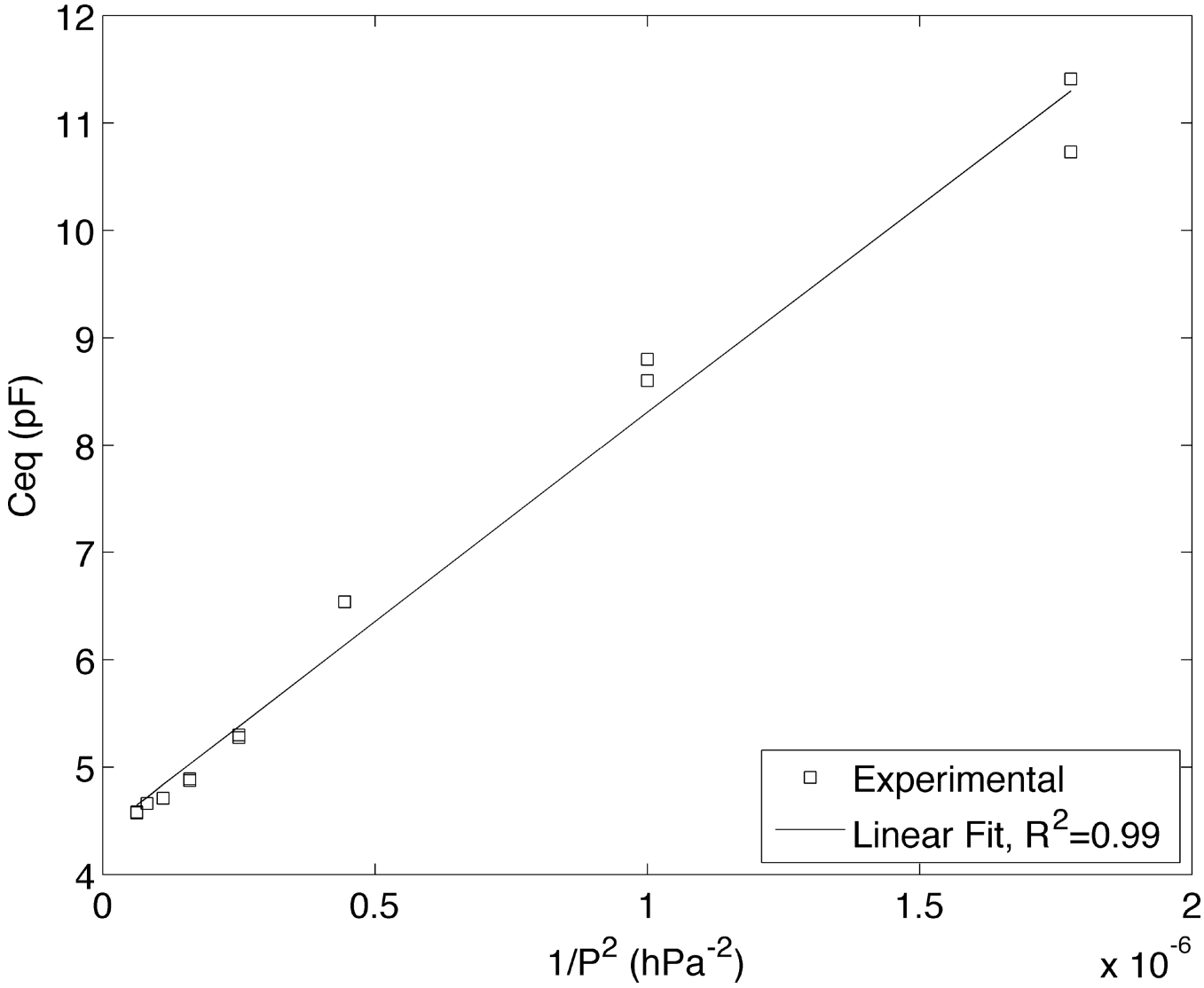

Figure 5.
The equivalent CNP's capacitance C_{eq} as a function of P^{-2}, where P is the control pressure. The symbols and the line represent, respectively, experimental data and the best linear fit.